Supporting information to

Hydrothermal synthesis of bi-functional nanostructured manganese tungstate catalysts for selective oxidation

Xuan Li,[a,b] Thomas Lunkenbein,[a] Jutta Kröhnert,[a] Verena Pfeifer,[a,c] Frank Girgsdies,[a] Frank Rosowski,[b,d] Robert Schlögl[a] and Annette Trunschke*[a]

[a.] *Department of Inorganic Chemistry, Fritz-Haber-Institut der Max-Planck-Gesellschaft, Faradayweg 4-6, 14195, Berlin, Germany*

[b.] *UniCat-BASF Joint Lab, Technische Universität Berlin, 10623, Berlin, Germany*

[c.] *Helmholtz-Zentrum Berlin für Materialien und Energie GmbH, Elektronenspeicherring BESSY II, Albert-Einstein-Str. 15, 12489 Berlin, Germany*

[d.] *BASF SE, Process Research and Chemical Engineering, Heterogeneous Catalysis, Carl-Bosch-Straße 38, 67056, Ludwigshafen, Germany*

* Correspondence author: trunschke@fhi-berlin.mpg.de.

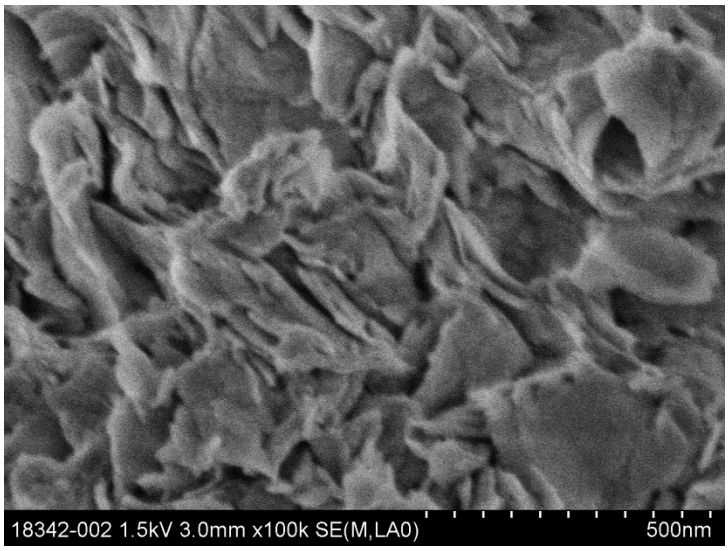

Figure S1. SEM image of the intermediate formed by reaction of manganese nitrate with sodium tungstate at room temperature.

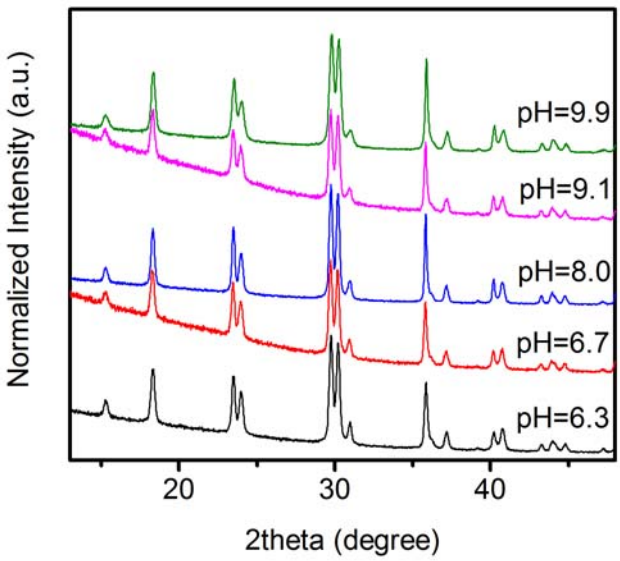

Figure S2. XRD patterns of the hydrothermal products; The pH of the starting solution is provided in the legend of the figure. For allocation of the corresponding final catalyst, please refer to Table 1 in the main text.

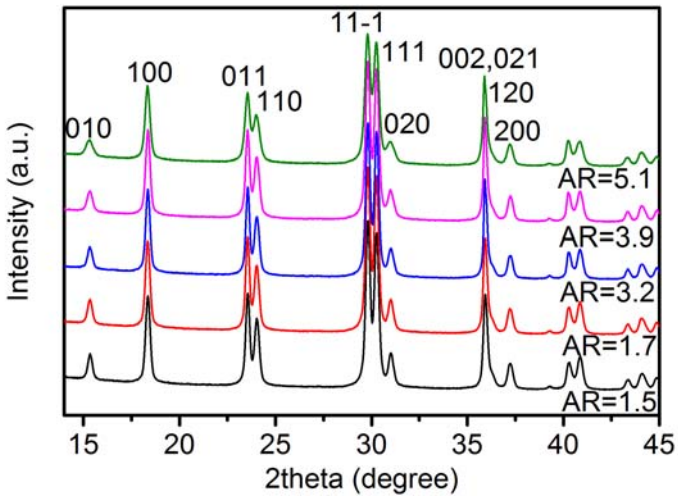

Figure S3. XRD patterns of the catalysts after activation by thermal treatment of the hydrothermal products in flowing Ar at 400°C.

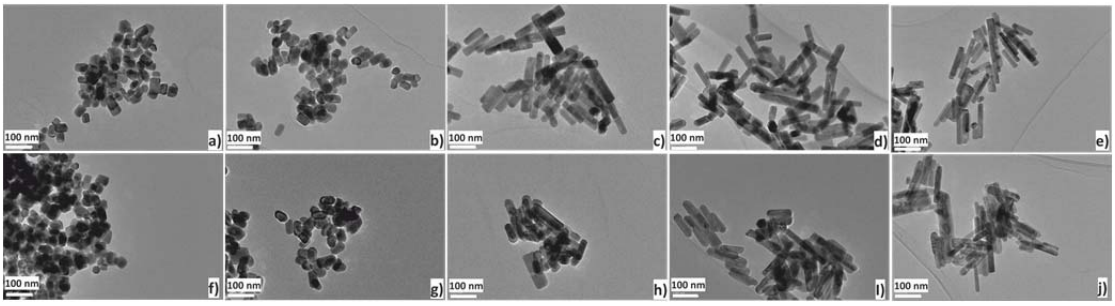

Figure S4.TEM micrographs of as-synthesized (top row) and at 400 °C thermally activated (bottom row) nanostructured $MnWO_4$ catalysts with different aspect ratio: 1.5 (a) and (e), 1.7 (b) and (g), 3.2 (c) and (h), 3.9 (d) and (i), 5.1 (e) and (j).

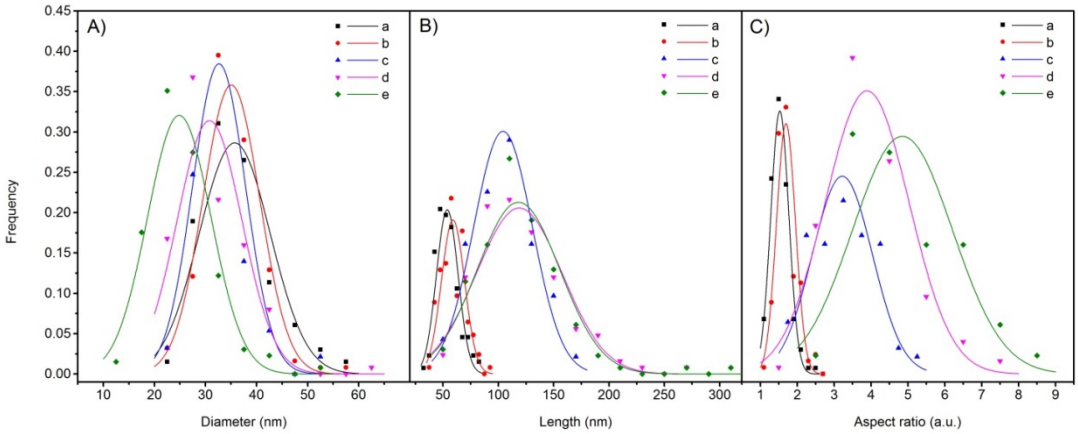

Figure S5. Distribution of A) diameter, B) length and C) aspect ratio of the nanostructured $MnWO_4$ catalysts after thermal treatment; In each plot, a, b, c, d, and e represent the catalysts AR1.5, AR1.7, AR3.2, AR3.9, and AR5.1, respectively.

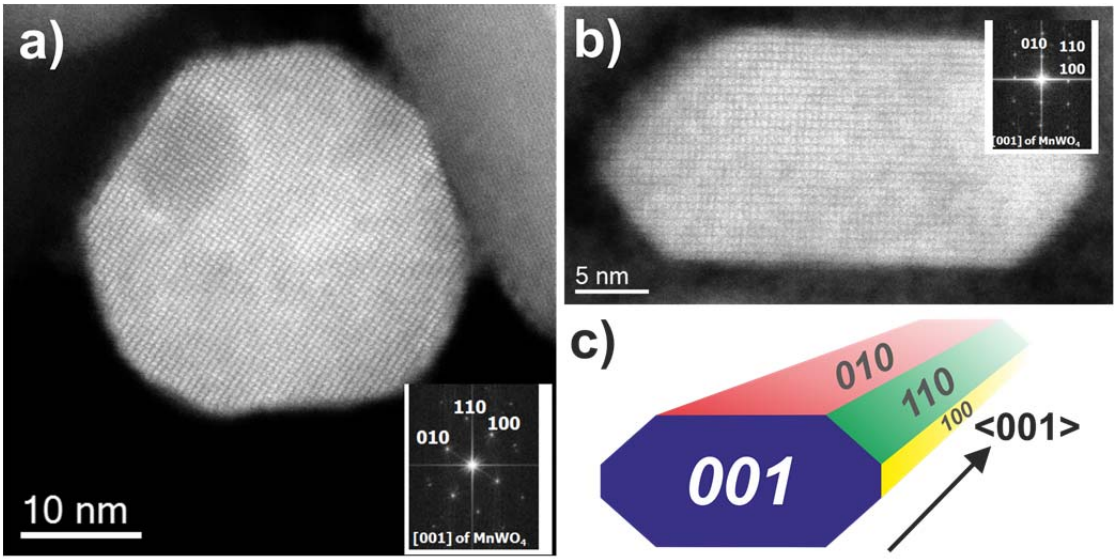

Figure S6. HAADF_STEM images of $MnWO_4$ nanoparticles viewed along <001> with different aspect ratios: a) AR1.5, b) AR5.1 and c) perspective model for a typical faceted nanoparticle.

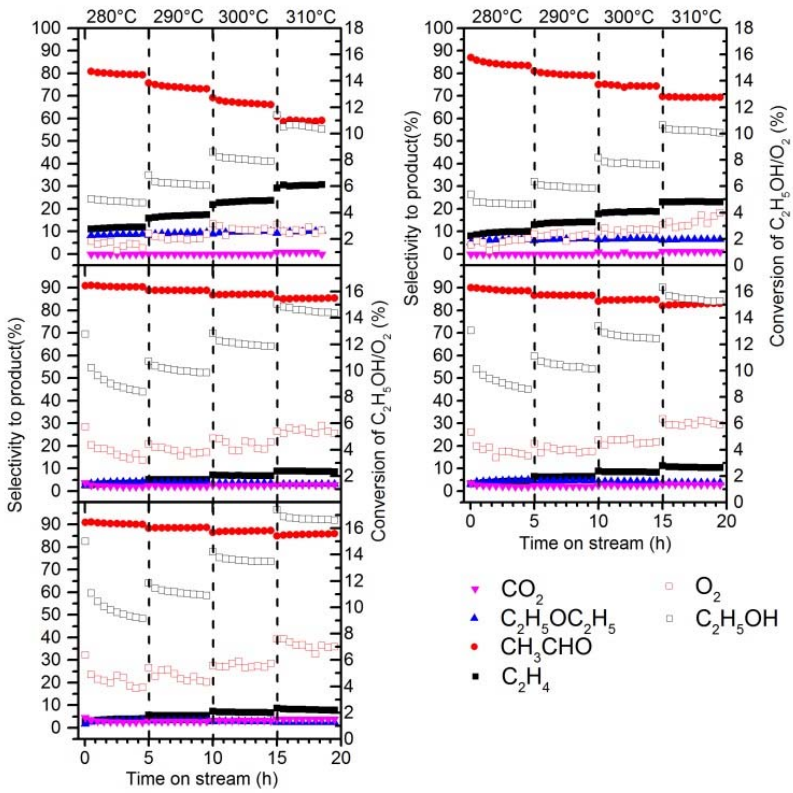

Figure S7. Catalytic performance of top-left) AR1.5, top-right) AR1.7, middle-left) AR3.2, middle-right) AR3.9, and bottom-left) AR5.1 sample in ethanol oxidation reaction at different temperatures; For reaction conditions see Experimental in the main text.

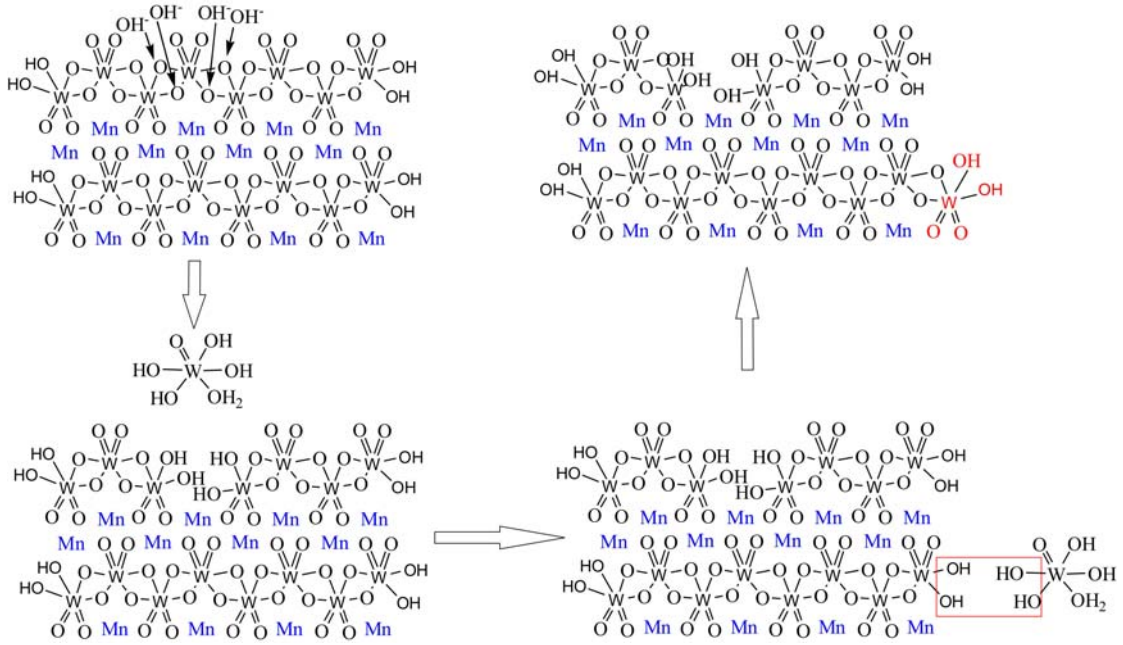

Figure S8. Schematic representation of the formation of W-OH groups at {001} planes during dissolution-recrystallization under hydrothermal conditions at 180°C.

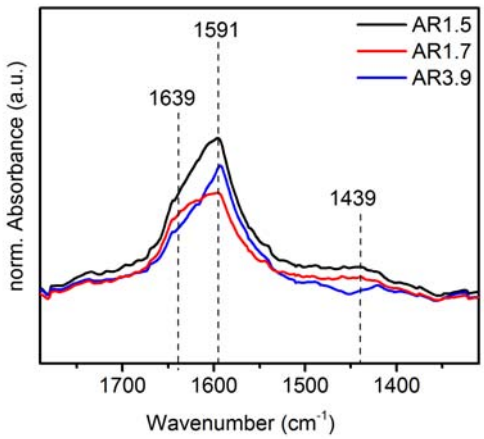

Figure S9. FTIR spectra of NH_3 adsorbed at the surface of the catalysts AR1.5, AR1.7, and AR3.9 after pretreatment at 300°C for 1h in vacuum; Adsorption of ammonia was performed at 40°C; The spectra have been recorded in presence of gas phase ammonia (*p*=6.508-7.042 mbar).

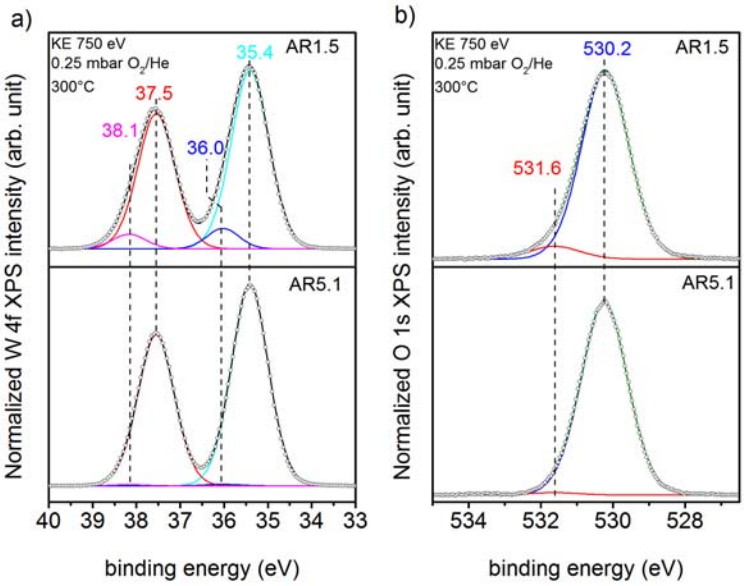

Figure S10. W 4f spectra (a)), and O 1s spectra (b)) of the catalysts AR1.5 and AR5.1 measured by synchrotron-based near ambient pressure X-ray photoemission spectroscopy (NAP-XPS) at an inelastic mean free path (IMFP) of ca. 1.6 nm in 0.25 mbar in O_2/He at a total gas flow of 4.2 sccm at 300°C.

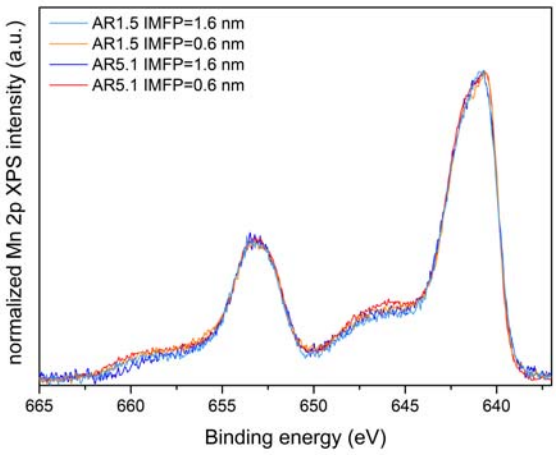

Figure S11. Mn 2p spectra of the catalysts AR1.5 and AR5.1 measured by synchrotron-based near ambient pressure X-ray photoemission spectroscopy (NAP-XPS) at an inelastic mean free path (IMFP) of ca. 0.6 nm (a) and 1.6 nm (b) in 0.25 mbar in O_2/He at a total gas flow of 4.2 sccm at 300°C.